

Article

Study on Convective Heat Transfer Characteristics of Supercritical Liquid Hydrogen in a U-Type Tube inside a Moderator

Weida Fu ^{1,2,3}, Yiping Lu ^{1,*}, Fei Shen ^{2,3}, Longwei Mei ^{2,3}, Songlin Wang ^{2,3}, Youlian Lu ^{2,3} , Lingbo Zhu ^{1,2,3}, Shinian Fu ^{2,3} and Jianfei Tong ^{2,3,4,*} 

¹ Department of Mechanical and Power Engineering, Harbin University of Science and Technology, Harbin 150080, China; fuwd@ihep.ac.cn (W.F.); zhulingbo@ihep.ac.cn (L.Z.)

² Institute of High Energy Physics, Chinese Academy of Sciences, Beijing 100049, China; shenf@ihep.ac.cn (F.S.); meilongwei@ihep.ac.cn (L.M.); wangsl@ihep.ac.cn (S.W.); luy1@ihep.ac.cn (Y.L.); fusrn@ihep.ac.cn (S.F.)

³ China Spallation Neutron Source Science Center, Dongguan 523803, China

⁴ School of Energy Science and Engineering, Harbin Institute of Technology, Harbin 150001, China

* Correspondence: luyiping@hrbust.edu.cn (Y.L.); tongjf@ihep.ac.cn (J.T.)

Abstract: The flow and heat transfer characteristics of supercritical fluid in a U-tube have an important influence on the safe operation of a moderator, and the variation of gravity direction is suitable for special working conditions of the moderator. In this study, the three-dimensional turbulence flow and heat transfers of supercritical liquid hydrogen in a U-tube were investigated at an Re number ranging from 16,425 to 54,750 under constant heat flux ($q = 80 \text{ kW/m}^2$). The total length of the U-tube was 1725 mm, which had an entrance length L/D of 23, with the inner diameter and wall thickness of $D \times \delta = 10 \times 2 \text{ mm}$. The finite volume method was adopted, and the grid independence was verified by the grid convergence index (GCI). The calculation results of three turbulence models (SST $k-w$, RNG $k-\epsilon$, Standard $k-\epsilon$) were compared with the corresponding experimental data to obtain the turbulence model with the smallest error. The convective heat transfer characteristics with different values of heat flux ($q = 30 \text{ kW/m}^2 \sim 100 \text{ kW/m}^2$), mass flow ($G = 3 \text{ g/s} \sim 10 \text{ g/s}$), and gravity (g_x, g_y, g_z) were compared. Meanwhile, the heat transfer characteristics of supercritical liquid and conventional liquid hydrogen were compared. The results show that Nu increased from 5 g/s to 10 g/s by 56.6%, and mass flow rate had a greater impact on the variation of Nu ; when gravity direction was consistent with the flow direction of liquid hydrogen (g_x direction), the Nu number inside the channel was 4.21% and 5.56% higher than that in g_y and g_z direction, respectively. Supercritical liquid hydrogen has a stronger heat transfer ability than conventional liquid hydrogen, of which the Nu number is 16.7% higher. This study can provide useful guidance for the design of flow and heat transfer of supercritical liquid hydrogen in a U-tube and its application in moderators. Furthermore, it provides reference technical values for thermal safety and thermal management of the target station to ensure its safe and stable operation.

Keywords: neutron moderator; numerical method; supercritical liquid hydrogen; U-tube; convective heat transfer; gravity



Citation: Fu, W.; Lu, Y.; Shen, F.; Mei, L.; Wang, S.; Lu, Y.; Zhu, L.; Fu, S.; Tong, J. Study on Convective Heat Transfer Characteristics of Supercritical Liquid Hydrogen in a U-Type Tube inside a Moderator. *Energies* **2022**, *15*, 3605. <https://doi.org/10.3390/en15103605>

Academic Editors: Xue Chen, Xian-long Meng, Chuang Sun and Jose A. Almendros-Ibanez

Received: 14 April 2022

Accepted: 13 May 2022

Published: 14 May 2022

Publisher's Note: MDPI stays neutral with regard to jurisdictional claims in published maps and institutional affiliations.



Copyright: © 2022 by the authors. Licensee MDPI, Basel, Switzerland. This article is an open access article distributed under the terms and conditions of the Creative Commons Attribution (CC BY) license (<https://creativecommons.org/licenses/by/4.0/>).

1. Introduction

In recent years, the rapid development of supercritical fluid technology has been widely used in aerospace, electrical engineering, nuclear technology, low temperatures, etc. The Chinese Spallation Neutron Source (CSNS), as the first spallation neutron source in China, has completed the first phase of its construction. In the process of using supercritical hydrogen as a moderator to improve neutron intensity and slow down neutron energy, it was proposed to use a composite moderator in the upcoming second phase project to provide more energy spectrum options for spectrometers [1]. The moderator is made by a combination of supercritical liquid hydrogen tubes and water. A U-tube can be used in

a moderator due to its compact structure and high heat transfer efficiency [2]. Under the condition of high thermal density and near the critical temperature, the physical properties of supercritical fluid will change dramatically, and its flow and heat transfer characteristics will be affected by different channel structures. Meanwhile, the thermodynamic process is very complex [3], so it is necessary to study the flow and heat transfer characteristics of supercritical liquid hydrogen in a U-tube [4]. Different domestic and foreign scholars have carried out relevant research on the flow and heat transfer characteristics of supercritical liquid hydrogen. For instance, Tomokazu et al. [5] carried out simulation experiments under different flow conditions to verify the feasibility of suppressing the local temperature rise to the range of 3 K in the design of a liquid hydrogen-cooled moderator. David [6] carried out experiments to improve the cooling efficiency of liquid hydrogen in a moderator. Hendricks and Simon [7] experimentally studied the flow and heat transfer characteristics of supercritical pressure hydrogen in elbows with different diameters and shapes under a uniform heat flux. Beech et al. [8] found that the flow and heat transfer phenomenon of supercritical hydrogen in elbow was affected by many factors, such as the physical property change and boundary conditions. The physical process was found to be complex, and it was difficult to summarize a universal phenomenon from limited experimental conditions. Zhou and Ji [9] simulated the flow and heat transfer of supercritical hydrogen in a 180° elbow. It was found that heat transfer outside the elbow was strengthened and that inside deteriorated.

In addition to supercritical liquid hydrogen, supercritical water and supercritical nitrogen [10,11] are also hot research topics. Many scholars have conducted numerical simulations based on different types of pipes, such as spiral pipes, loops and vertical circular pipes [12–14]. Wang et al. [15] carried out an experimental study on the heat transfer of aviation kerosene in a U-tube under supercritical pressure. Wu [16] discussed the effects of four factors, including inlet temperature, heat flux, inlet pressure and inlet mass flow, on the flow and heat transfer process of supercritical n-decane in a rectangular straight pipe channel. Yu [17] studied the flow and heat transfer characteristics of a supercritical CO₂–propane binary mixture. The results showed that the heat transfer coefficient of the CO₂–propane mixture decreases with increase of heat flux at same temperature.

There are few studies on the heat transfer characteristics of supercritical liquid hydrogen tubes with a U-shape and constant heat flux on the outer wall. The application value of a supercritical liquid hydrogen tube for a moderator and attention of the neutron source were considered in this study. In the current work, the flow characteristics of supercritical liquid hydrogen in a U-shaped tube were investigated, especially the heat transfer research when gravity direction changes in extreme conditions. Nowadays, the operating conditions of CSNS will be upgraded to $G = 30 \text{ g/s}$, $q = 500 \text{ kW/m}^2$. Therefore, this work is of great significance for the thermal safety and emergency response of the target station.

2. Numerical Simulation

2.1. Physical Model

The U-tube geometry model is shown in Figure 1. According to a previous study of a spallation neutron source for moderators, most pipelines inside moderators can adopt a small diameter. In this study, the spatial direction of the U-tube was vertical, and the fluid flow direction was consistent with the gravity direction (g_x). The total length of the U-tube was 1725 mm, with an inner diameter and wall thickness of $D \times \delta = 10 \text{ mm} \times 2 \text{ mm}$. The curvature radius of the elbow was $R = 27 \text{ mm}$, and the length of the heating section was $L = L_1 + L_2 + L_3 = 525 \text{ mm}$. To weaken the inlet section effect and outlet reflux phenomenon, before and after the heating section of the U-tube, namely, the inlet and outlet were respectively set with a 600 mm adiabatic inlet section and a 600 mm adiabatic outlet section.

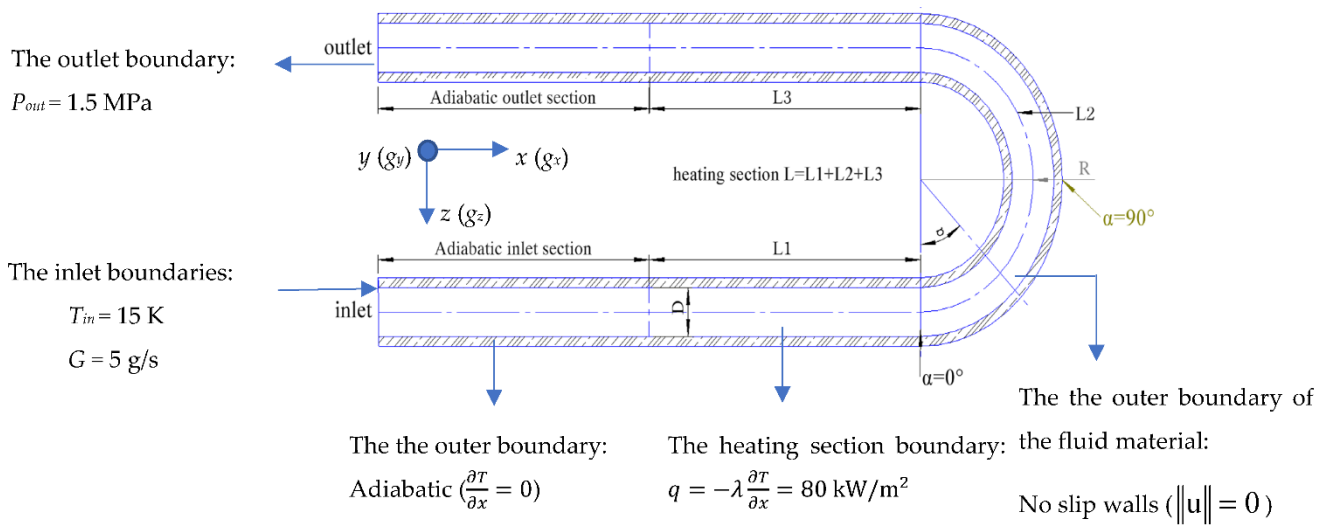


Figure 1. U-type tube model.

2.2. Meshing

The calculation domain of the U-tube was established and meshed. As shown in Figure 2, the upper half grid diagram of the computational domain in the $yo z$ direction and xoz section direction of the horizontal tube inlet were presented. Considering that the physical parameters of fluid in the boundary layer region near the wall will change dramatically, the flow and heat transfer characteristics were relatively complex, and the grid near the wall was encrypted. Through the finer grid, the flow and temperature field around the U-tube were investigated in detail. In this work, the enhanced wall function ($y^+ < 1$) was used to divide the grid, which has certain advantages for studying the heat transfer and flow conditions of the wall.

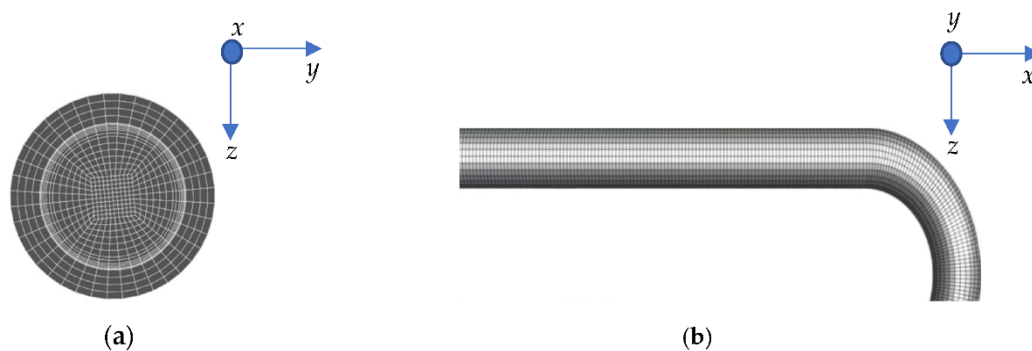


Figure 2. (a) Cross $yo z$ section grid; (b) xoz section grid.

2.3. Governing Equations

In the current work, it was assumed that fluid flow was in a steady turbulent state and did not have an internal heat source.

The continuity, momentum, and energy conservation equations were described as follows [18]:

The continuity equation:

$$\nabla \cdot (\rho \vec{u}) = 0 \tag{1}$$

The momentum equation:

$$\nabla \cdot (\rho u \vec{u}) = -\frac{\partial p}{\partial x} + \frac{\partial \tau_{xx}}{\partial x} + \frac{\partial \tau_{yx}}{\partial y} + \frac{\partial \tau_{zx}}{\partial z} + \rho f_x \nabla \cdot (\rho v \vec{u}) = -\frac{\partial p}{\partial y} + \frac{\partial \tau_{xy}}{\partial x} + \frac{\partial \tau_{yy}}{\partial y} + \frac{\partial \tau_{zy}}{\partial z} + \rho f_y \nabla \cdot (\rho w \vec{u}) = -\frac{\partial p}{\partial z} + \frac{\partial \tau_{xz}}{\partial x} + \frac{\partial \tau_{yz}}{\partial y} + \frac{\partial \tau_{zz}}{\partial z} + \rho f_z \tag{2}$$

The energy equation:

$$\nabla \cdot [(\rho E + P)\vec{u}] = \nabla \cdot (\lambda_{eff} \nabla T - (\tau_{eff} \cdot \vec{u})) + S_h \quad (3)$$

where ρ is density; \vec{u} is the velocity vector; u, v, w are components of velocity \vec{u} ; τ is the stress tensor; p is the bulk fluid pressure; λ is thermal conductivity; T is bulk fluid temperature; E is total energy; P is static pressure; τ_{eff} is shear stress; λ_{eff} is effective thermal conductivity; S_h is volumetric heat source.

In this study, the Re value under working conditions was much higher than its critical value, so the flow was in a turbulent state. During the simulation, the standard $k-\varepsilon$ turbulence model was selected to describe the turbulent flow [19].

The transport equations are described as follows:

$$\frac{\partial}{\partial x_i} (\rho k \vec{u}) = \frac{\partial}{\partial x_j} \left[\left(\mu + \frac{\mu_t}{\sigma_k} \right) \frac{\partial k}{\partial x_j} \right] + G_K + G_b - \rho \varepsilon - Y_M + S_k \quad (4)$$

$$\frac{\partial}{\partial x_i} (\rho \varepsilon \vec{u}) = \frac{\partial}{\partial x_j} \left[\left(\mu + \frac{\mu_t}{\sigma_\varepsilon} \right) \frac{\partial \varepsilon}{\partial x_j} \right] + C_{1\varepsilon} \frac{\varepsilon}{k} (G_K + C_{3\varepsilon} G_b) - C_{2\varepsilon} \rho \frac{\varepsilon^2}{k} + S_\varepsilon \quad (5)$$

where,

$$\mu_t = \rho C_\mu \frac{k^2}{\varepsilon} \quad (6)$$

where G_k represents the generation of turbulence kinetic energy due to the mean velocity gradients, G_b is the generation of turbulence kinetic energy due to buoyancy, Y_M represents the contribution of the fluctuating dilatation incompressible turbulence to the overall dissipation rate, μ is dynamic viscosity, μ_t is turbulent viscosity, k is turbulent kinetic energy, ε is the dissipation rate of turbulent kinetic energy and E is total energy. σ_k and σ_ε are the turbulent Prandtl numbers for k and ε , respectively. S_k and S_ε are source terms. The model constants $C_{1\varepsilon}$, $C_{2\varepsilon}$, C_μ , σ_k , σ_ε had the following default values: $C_{1\varepsilon} = 1.44$, $C_{2\varepsilon} = 1.92$, $C_\mu = 0.09$, $\sigma_k = 1.0$, $\sigma_\varepsilon = 1.3$ [20].

2.4. Data Reduction Method

The dimensionless independent parameter Re was obtained by Equation,

$$Re = \frac{\rho u D}{\mu} \quad (7)$$

The local Nusselt number Nu was defined as:

$$Nu = \frac{hD}{\lambda} \quad (8)$$

where D is the hydraulic tube diameter, and h is the local heat transfer coefficient.

The local heat transfer coefficient equation was as follows:

$$h = \frac{q_u}{T_w - T_b}, T_b = f(H_b, P), H_b = \frac{\int A \rho u H dA}{\int A \rho u dA} \quad (9)$$

where q_u is the local heat flux of wall, T_w is the averaging temperature wall, T_b is the bulk temperature of fluid, u is the axial velocity of the fluid, A is the cross-sectional area of the pipe and H is the bulk liquid enthalpy.

2.5. Calculation Conditions

In this study, ANSYS CFX 2021 software was used to conduct a numerical simulation of heat transfer characteristics of supercritical liquid hydrogen in U-shaped tubes. The

Semi-Implicit Method for Pressure-Linked Equations of pressure coupled equations was selected. The finite volume method was used to discrete the control equation and other equations in which the second-order upwind was selected for the discretization scheme. The root mean square (RMS) value of the residual value was set to 10^{-6} , and the number of iterations was set to 10,000 times, until a stable independent convergence solution was obtained. The relaxation factors were all based on the default value. In the residual setting, except that the energy equation term was less than 10^{-6} , the variables were less than 10^{-4} .

The boundary conditions of the model were set to be simulated, including its fluid domain and solid domain.

1. Boundary condition setting: Firstly, the reference working condition was established, As shown in Figure 1, the gravity direction was the positive direction of the x -axis, and constant heat flow q was used in wall of the heating section. The boundary conditions are shown in the following.

$$q = -\lambda \frac{\partial T}{\partial x} = 80 \frac{\text{kW}}{\text{m}^2}, G = 5 \text{ g/s}, g_x = 9.8 \text{ m/s} \quad (10)$$

$$T_{in} = 15 \text{ K}, P_{out} = 1.5 \text{ MPa} \quad (11)$$

2. Parameter settings of physical properties: Thermophysical properties of liquid hydrogen under supercritical conditions can be obtained from data provided by the National Institutes of Standards and Technology (NIST) [21]. The physical properties of liquid hydrogen can be regarded as a single value function of temperature. The corresponding thermal properties were inputted through the piecewise-linear interpolation function of CFX 2021. In this work, GASPAC software was used to calculate the thermophysical parameters of supercritical fluid hydrogen. When the temperature was inputted, the thermophysical parameters of the corresponding fluid were obtained, such as λ , c_p , μ , ρ . The temperature range selected in this study was 15 K~40 K. The thermophysical parameters of supercritical liquid hydrogen were plotted by the obtained thermophysical parameters, as shown in Figure 3.
3. As shown in Figure 3, the thermophysical properties of liquid hydrogen change with temperature at $P = 1.5 \text{ MPa}$. For supercritical fluids, they were near the pseudo-critical temperature (the temperature corresponding to the maximum specific heat capacity of fluid at supercritical constant temperature). The physical properties of fluid will change sharply, which will affect the heat transfer of fluid. In general, the critical pressure and temperature of liquid hydrogen are 1.29 MPa and 33.15 K, respectively. It can be seen from Figure 3 that density, ρ , and dynamic viscosity, μ , both showed a downward trend with the increase in temperature and, finally, tended to converge. The changing trend of specific heat, c_p , and thermal conductivity, λ , was similar. Still, the changing trend of specific heat, c_p , was more significant, which is not conducive to the stability of liquid hydrogen in heat transfer.

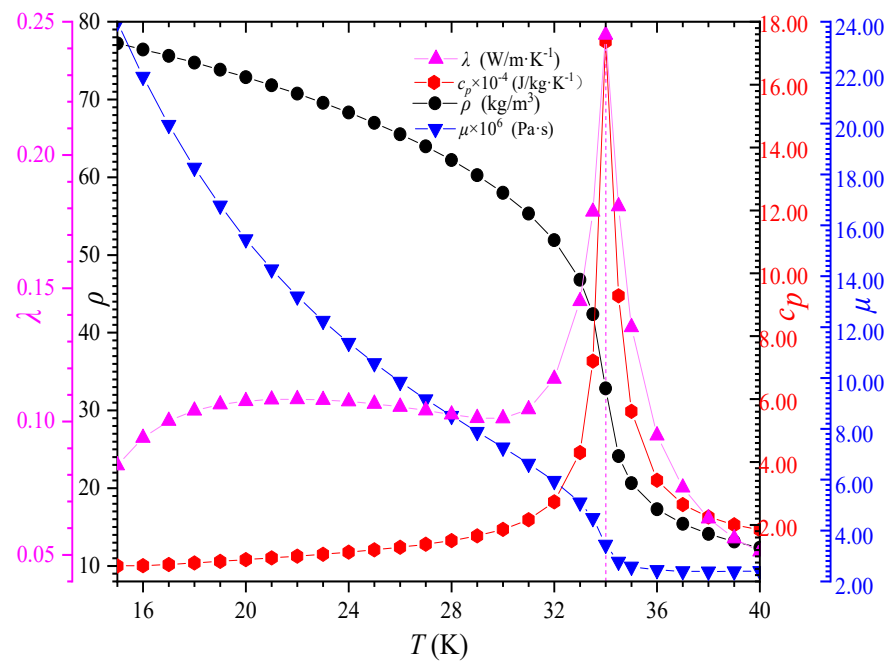


Figure 3. Curve of thermophysical properties of liquid hydrogen with temperature.

3. Results and Discussion

3.1. Verification of Grid Independence

The quality and quantity of grids have a significant influence on calculation results, so it is necessary to verify grid independence. In order to ensure the reliability of the near-wall calculation, the enhanced wall function was selected, and the y^+ value should have been less than 1. In this study, five groups of grids were used to test the independence of grids. The maximum temperature of liquid hydrogen, the average flow rate and the maximum temperature of the outlet were monitored. As shown in Figure 4, simulation results of different grids are presented, among which five groups of grids were 0.56, 1.02, 1.53, 1.98 and 2.41 million, respectively. As the number of grids increased from 1.98 million, the trend of the three groups of variables tended to be gentle, and a convergence solution could be obtained. Considering the calculation accuracy and efficiency, the grid number of 1.98 million was selected for this study to ensure that the calculation results had grid independence.

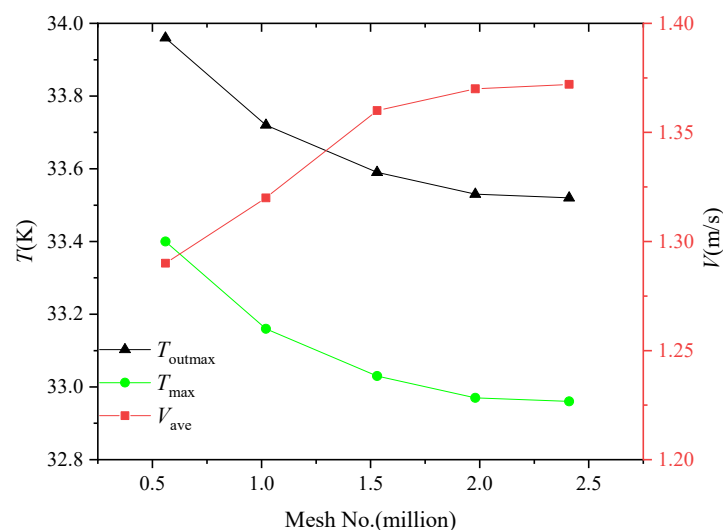


Figure 4. Grid independence validation of CHM.

The grid convergence index (GCI) [22] was defined as:

$$GCI = F_s \frac{|\varepsilon|}{r^p - 1} \varepsilon = \frac{f_1 - f_2}{f} \quad (12)$$

$$r_{k,k+1} = \sqrt[3]{\frac{N_{k+1}}{N_k}} \quad (13)$$

where F_s is the safety factor value of 1.25, f is the maximum values of f_1 and f_2 , f_1 and f_2 are the outlet temperature values, N_k is the number of grids and p is the convergence accuracy, which is 1.97. GCI_{12} was 0.75%, GCI_{23} was 2.76%, GCI_{34} was 0.81% and GCI_{45} was 1.23%, and the values were less than 3%, indicating that the numerical simulation results were independent of number of grids. Considering the calculation accuracy and efficiency, the fourth data group was sufficient to ensure grid independence of the calculation results.

3.2. Sensitivity Analysis of Turbulence Model

To prove that the selected turbulence model well-described the flow of supercritical liquid hydrogen in the tube, a variety of turbulence models were chosen to compare with the experimental data as references at the same boundary conditions [23]. In the experiment, the thermal thermocouple and automatic voltage digitizing system were used to measure the pipe wall temperature and fluid temperature, respectively. In the condition of $G = 4.5 \text{ kg/m}^2 - 45 \text{ kg/m}^2$, $P = 1 \text{ MPa} - 5 \text{ MPa}$, 12 groups of data were collected to compare the results of liquid hydrogen in the supercritical state and pressure critical state. The specific model was a circular tube with a diameter of 8.51 mm and a length of 0.9144 mm. The inlet flow rate of supercritical liquid hydrogen was 4.5 kg/m^2 , and the inlet temperature and pressure were 25.33 K and 4.947 MPa, respectively.

It can be seen from Figure 5 that the partition trends of the supercritical liquid hydrogen temperature and tube wall temperature calculated by different turbulence models were in good agreement with the experimental results. However, there were still some differences between them. By observing and analyzing the distribution of wall temperature and liquid hydrogen temperature, it was found that the standard $k-\varepsilon$ model had the best consistency. The error of the liquid hydrogen temperature distribution was not more than 5%, and the maximum error between the experimental value and simulation value were within 20%. The overall temperature distribution of other models was lower than the experimental data, so the standard $k-\varepsilon$ model was finally used as the turbulence model in the current work.

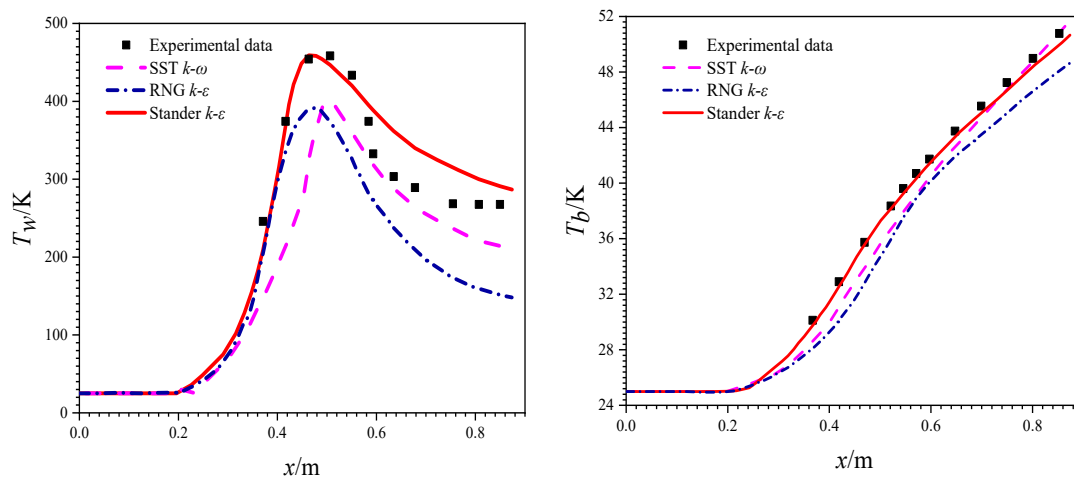


Figure 5. Sensitivity analysis of the turbulence model.

3.3. Analysis of Heat Transfer Characteristics under Benchmark Conditions

3.3.1. Analysis of Longitudinal Temperature, Density and Velocity under the Reference Condition

As mentioned above, the reference operating parameters were $q = 80 \text{ kW/m}^2$, $G = 5 \text{ g/s}$ and $g_x = -9.8 \text{ m/s}^2$ to analyze the longitudinal and transverse velocity, temperature and density of the U-tube. Figure 6 is the distribution of velocity (a), temperature (b) and density (c) of xoy plane; the velocity streamline (positive along x -direction) (d) and the temperature iso-surface (e) in the computational domain. It can be seen from the diagram that liquid hydrogen flowed evenly before entering bending channel and separated after entering the bending pipe. A low temperature and high-density region were formed on the outer wall of the tube, and a high temperature and low-density region were formed on the inner wall of tube. Along the flow direction, the low-temperature zone was in front, and the high-temperature zone was in the back. Finally, in the back of the elbow, two regions produced a mixing phenomenon. The velocity distribution in the flow channel was different. In the first half of the bend, the velocity on the inner side was abruptly increased from 0.9 m/s to 1.2 m/s , while velocity on the outer side was decreased from 0.9 m/s to 0.8 m/s . In the latter half of the elbow, the inner flow velocity decreased gradually, while the outer flow velocity increased and was higher than the inner. The main reason was that liquid hydrogen was just entering elbow. Due to the sudden emergence of the centrifugal force, the fluid inside the tube had a lateral displacement from inside to outside and produced fluid extrusion. The flow velocity of the outside fluid was reduced under extrusion, while space inside became larger, and flow velocity increased significantly. Then, with the flow of fluid, the distribution was gradually uniform. Under the action of centrifugal force, the velocity of the outer fluid was gradually accelerated, and the velocity of the inner fluid was slower. Figure 7 illustrates the distribution of the temperature, density, and secondary flow trace on the different cross-sections of the bent tube. When the fluid flowed into the elbow, the lateral flow became obvious, and the Dean vortex was formed. The secondary flow on the cross-section took the cold fluid from the core to the outside of the U-tube elbow, and the heated fluid on the outside (near the wall) flowed along the wall to the inner-side and then reached the center of the pipe. The traces near the wall generated by the buoyancy force moved up gradually. In contrast, the Dean traces generated by the centrifugal force moved down gradually, and all of them could be seen in the $\alpha = 120^\circ$ section. In addition, the thermal boundary layer became thinner and disappeared during circulation, and there was a sudden temperature difference between the wall and the fluid near the wall. Because under the influence of the enhanced secondary flow, a thin layer of fluid nearby may absorb more heat, and the bulk temperature of supercritical hydrogen in this layer may have increased rapidly due to the significant decrease in density. To summarize, the secondary flow phenomenon could conduce thinning of the boundary layer of supercritical hydrogen, thus enhancing heat transfer.

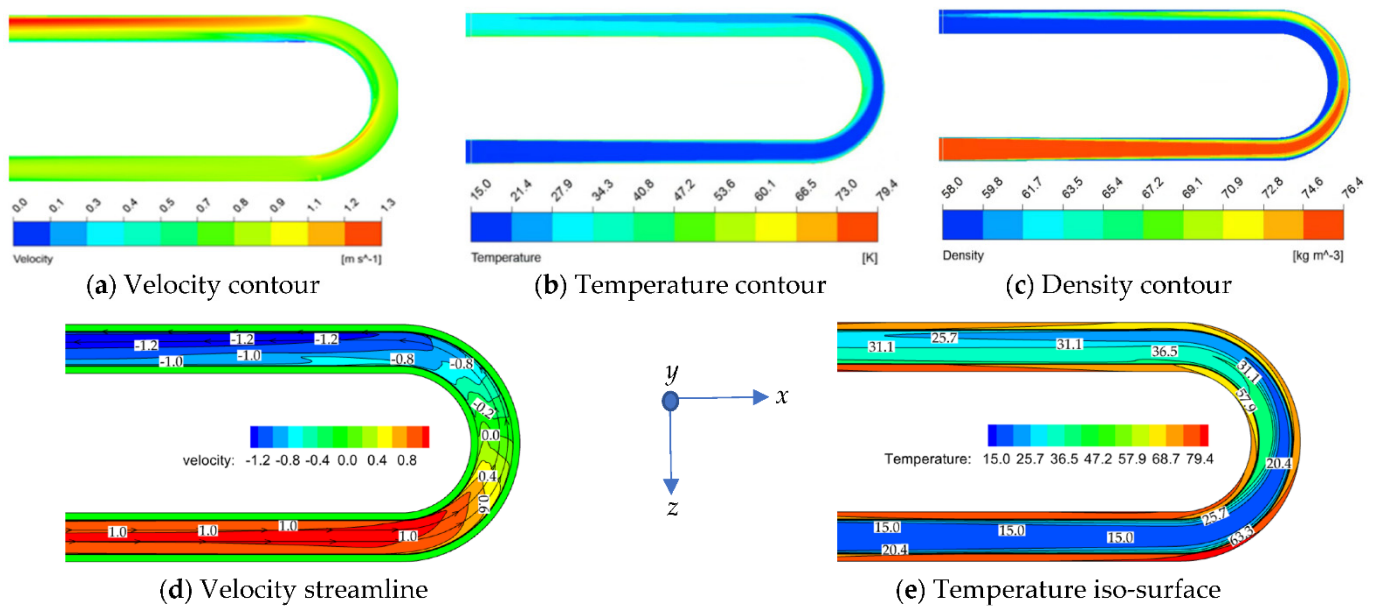


Figure 6. Velocity, temperature and density contours of xoy plane in U-type tube heating section.

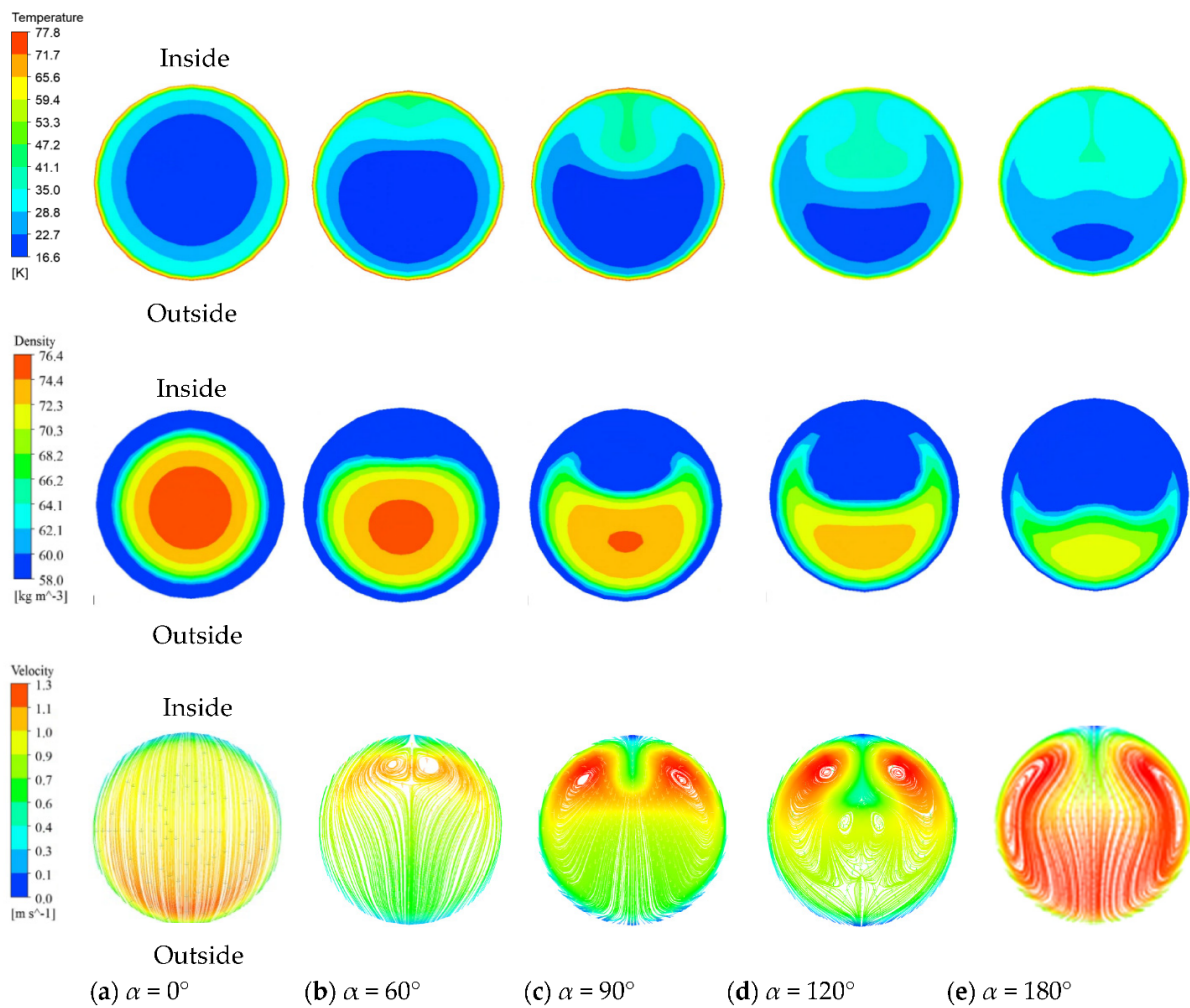


Figure 7. Temperature, density and velocity contours on the α section of the bend pipe with different bending angles.

3.3.2. Analysis of Section Temperature, Density and Velocity at the Bend Pipe under the Reference Condition

Figure 7 shows the temperature, density and trace contour of the calculated elbow on the cross-section of α (0° , 60° , 90° , 120° , 180°) at different angles. In general, all contour images exhibited left–right symmetry. From Figure 7a, it can be seen that temperature and density distribution inside and outside the flow channel were the same near the entrance section of the elbow at $\alpha = 0^\circ$, which was consistent with the theoretical analysis. The temperature and density contour showed a concave shape in $\alpha = 90^\circ$ – 120° . It could be seen from the temperature distribution contour that after entering the elbow section, the temperature distribution was closely related to the velocity distribution, and the velocity field determined the temperature field. As mentioned above, the flow rate of liquid hydrogen inside the pipeline was lower than that of the outside, which led to the heat transfer capacity of the inside pipeline being weaker than that of the outside. Therefore, the temperature of liquid hydrogen inside the pipeline was higher than that outside. It can be seen from the trace diagram that the secondary flow double vortex generated by the combined action of the centrifugal force and buoyancy appeared at $\alpha = 60^\circ$, which was located inside, and the vortex area as well as the velocity increased with the increase of the α angle. From $\alpha = 90$ – 180° , it can be seen that with the increase in angle, the vortex near the wall and internal vortex gradually move from the inside to the outside. At $\alpha = 180^\circ$, due to the disappearance of centrifugal force, only the secondary flow vortex generated by buoyancy was left, and the vortex at this time accounted for most of the region. The temperature, density and velocity distribution characteristics of liquid hydrogen in the elbow can be ultimately observed in Figures 6 and 7.

3.3.3. Analysis of T_w , h and Nu in the Tube

Figure 8 shows the change of T_w , h and Nu with the direction of L/D when supercritical liquid hydrogen and conventional liquid hydrogen are heated in a U-tube. Point lines at $L/D = 22$, 26 and 30 indicate the upstream below the inlet, mid-point and downstream elbow outlet of the U-type. As shown in the figure, the overall trends of the two working fluids were similar. It could be found that T_w at the straight pipe section increased continuously along the flow direction of liquid hydrogen inside the pipe. After liquid hydrogen entered the elbow section ($\alpha = 0^\circ$), the wall temperature, h and Nu curves all showed inflection points. The wall temperature gradually decreased from 79° to 63.8° , and the temperature difference of convective heat transfer increased. The variation trends of convective heat transfer coefficients h and Nu were opposite to the wall temperature. This was mainly due to the centrifugal force, resulting in a secondary flow, so that the velocity of liquid hydrogen in the outer tube was higher than that of the inner tube. It can be seen from Figure 8 that at the elbow ($\alpha = 0^\circ$ – 180°), h and Nu between liquid hydrogen and the pipe wall increased significantly. More specifically, the heat transfer was strengthened. Finally, at the position flowing out of the elbow ($\alpha = 180^\circ$, $L/D = 30$), the centrifugal force inside the pipe disappeared, and the curve showed a turning point. Nu and h gradually decreased with the increase of the boundary layer. The temperature near the wall of the fluid slowly increased, and heat transfer deteriorated. During the flow of the fluid in the upstream and downstream straight pipes ($L/D = 0$ – 22 , 30 – 40), the thermophysical properties of supercritical liquid hydrogen changed with temperature. Since Nu is the function of h and λ , the trends of Nu and h were not completely consistent. Because the heat transfer intensity determined the number of T_w , T_w presents a completely opposite trend with h and Nu , which directly reflects the heat transfer characteristics of the U-tube. The secondary flow generated by the centrifugal force at the elbow was dominant, and both mutations occurred. At the $L/D = 23$ to 30 position, the numerical mutation phenomenon appeared and reached the peak, respectively. The main reason is that this position was located in the inlet and outlet area of the elbow. At this time, the centrifugal force and the physical parameters of the supercritical liquid hydrogen were particularly violent, so the numerical value changed drastically. Due to the fact that the thermophysical properties

of conventional liquid hydrogen do not change with temperature, the numerical changes at the elbow were not obvious. The overall trend of the Nu curve was similar to h , and the peak point of Nu and h appeared in the same position. Nu could accurately reflect the heat transfer of liquid hydrogen in the U-tube, which is the same as that of supercritical carbon dioxide [24]. For conventional liquid hydrogen, its thermophysical properties do not change with temperature. Therefore, compared with supercritical liquid hydrogen, the change of T_w , h and Nu in the conventional liquid hydrogen flow in a U-tube was relatively flat, and the heat transfer ability was also weaker.

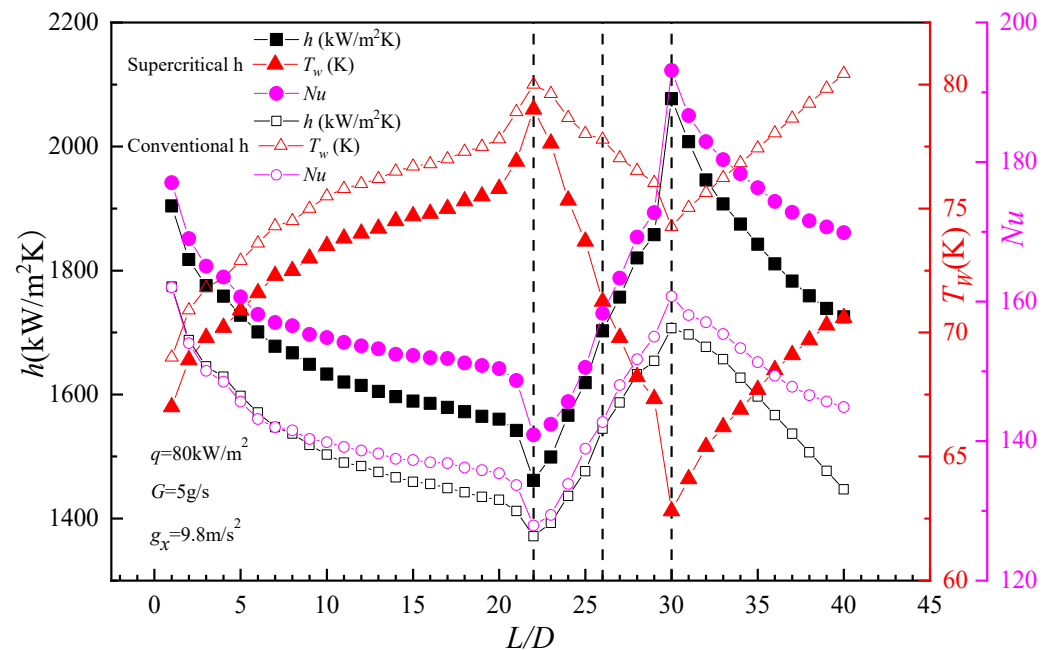


Figure 8. Variation of T_w , h and Nu with L/D .

3.4. Analysis of the Average Nu and Minimum Nu under Different Working Conditions

It was found that based on the above research, when the inlet mass flow rate G of liquid hydrogen in a single change tube was 3~10 (g/s), the heat flux q of the tube wall was 30~100 (kW/m²). The variation of T_w , h and Nu with L/D was similar to the above variables. The difference was as follows: After entering the elbow section, with the increase of heat flux, the valley point of T_w shifted to the left, and the peak point of Nu gradually shifted to left, which corresponded to the valley point of the wall temperature. The average and minimum Nu curves for above G range of 3~10 (g/s) and the tube wall heat flux q range of 30~100 (kW/m²) are shown in Figure 9a,b. At the same time, it was compared with conventional liquid hydrogen, and the final results of the two fluids were compared and analyzed.

As shown in Figure 9, under different Re and heat flux densities, the variation trends of average Nu and minimum Nu in two different fluids were the same. The inlet flow $G = 5$ g/s and heat flux $q = 80$ kW/m² were taken as reference conditions for analysis. It can be seen from Figure 9a that heat flux was 80 kW/m², as the reference condition for the analysis. The average Nu and the minimum Nu decreased from 5 g/s to 3 g/s by 25.9% and 26.8%, respectively, and increased from 5 g/s to 10 g/s by 56.6% and 58.9%, respectively. According to Figure 9b, when the mass flow rate was 5 g/s, the average Nu and minimum Nu decreased by 13.4% and 14.6%, respectively, from 80 kW/m² to 30 kW/m² and increase by 3.5% and 3.7%, respectively, from 80 kW/m² to 100 kW/m². It can be found from Figure 9a,b that the average Nu and minimum Nu of conventional liquid hydrogen were smaller than those of supercritical liquid hydrogen. Based on the above conclusions, it can be inferred that the heat transfer ability of supercritical liquid hydrogen is stronger than conventional liquid hydrogen. For a straight pipe, when Re reaches 1×10^5 , it tends to be almost constant, but for an elbow pipe ($\alpha = 0^\circ \sim 180^\circ$), Nu increases with the increase of the Reynolds number and heat flux,

showing an approximate linear upward trend. To sum up, the Reynolds number has a greater influence on the change of Nu .

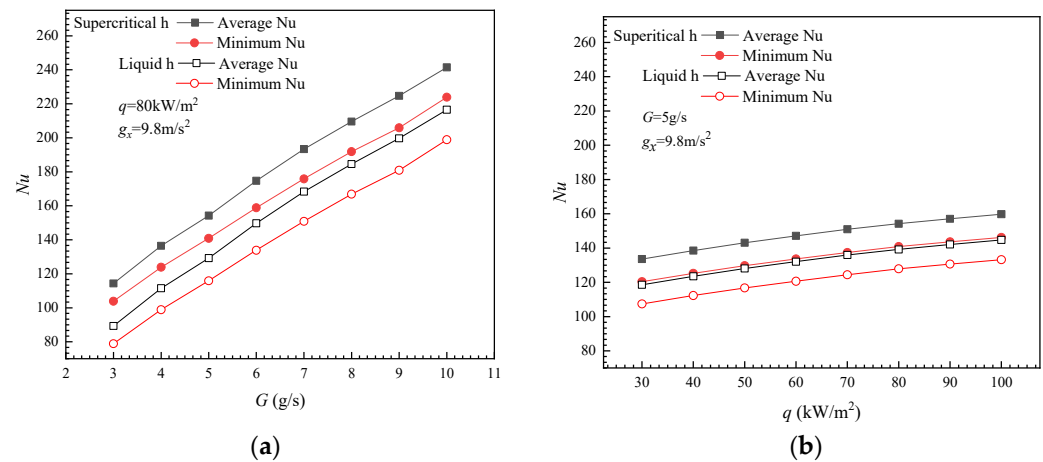


Figure 9. Comparison of average Nu and minimum Nu of supercritical and traditional liquid hydrogen under different conditions of G and q (a,b).

3.5. Effect of Gravity Direction on Flow and Heat Transfer of Supercritical Liquid Hydrogen

In unique working conditions, disasters such as earthquakes may have occurred, and the gravity direction of the U-tube where the supercritical liquid hydrogen is located will change accordingly, which has a particular impact on the research of a spallation neutron source. Therefore, to explore the influence of different gravity directions on low and heat transfer of supercritical liquid hydrogen in U-tube, the benchmark conditions were established: $G = 5 \text{ g/s}$, $q = 80 \text{ kW}$.

As shown in Figure 10a,b, point lines at $L/D = 22$, 26 and 30 indicate the position of upstream elbow inlet, mid-point and downstream elbow outlet of the U-type. Figure 10c shows the direction of gravity. When gravity directions were $(g_x = -9.8 \text{ m/s}^2, 0, 0)$, $(0, g_y = -9.8 \text{ m/s}^2, 0)$, and $(0, 0, g_z = -9.8 \text{ m/s}^2)$, respectively, T_w and Nu changed with the direction of L/D , where $(g_x = -9.8 \text{ m/s}^2, 0, 0)$ were taken as condition parameters of the above study. It can be seen from Figure 10a that wall temperature was the highest when gravity was along the z -direction and the smallest when gravity was along the x -direction. When fluid flowed in the flow channel, the wall temperature decreased with the increase of gravity, and wall temperature decreased gradually after fluid entered the elbow section. The wall temperature rose as the fluid left the elbow. The numerical mutation at the elbow was due to the thermal properties of supercritical hydrogen and the centrifugal force, which is mentioned above.

It can be seen from Figure 10b that as gravity changed from the z -axis direction to the x -axis direction, Nu also increased, and the peak point of the Nu curve corresponded to the valley point of the wall temperature change curve. The main reason was that with the flow process of supercritical liquid hydrogen in the channel, there is a temperature difference in the channel to form a density difference. Under the action of gravity, buoyancy is formed in the U-tube and can produce a secondary flow to strengthen the heat transfer in the channel. In the flow channel, the direction of buoyancy is directly related to heat transfer ability. When buoyancy is in the radial direction, it is conducive to convective heat transfer. When fluid is in the tangential direction, it will lead to the deterioration of heat transfer [25]. When gravity is along x -axis, the same as the flow direction of liquid hydrogen, the heat transfer capacity was the strongest, and Nu was the largest. When along the z -axis direction, the velocity and temperature distribution in the flow channel were unevenly distributed, which deteriorated the heat transfer and minimized Nu .

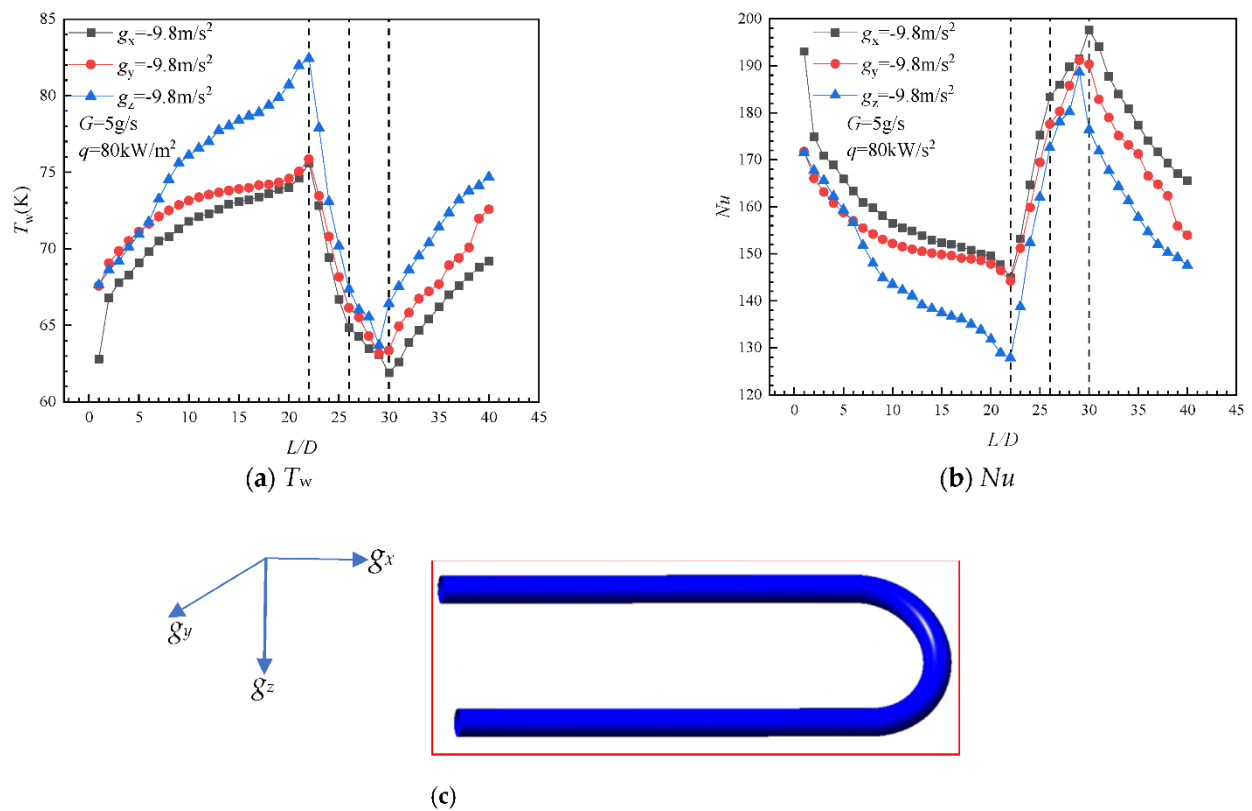


Figure 10. Variation of T_w , Nu with L/D under different gravity directions and gravity direction diagram.

4. Conclusions

The working conditions considered in this study, $G = 3 \text{ g/s} \sim 10 \text{ g/s}$ ($Re = 16,425 \sim 54,750$), $q = 30 \text{ kW/m}^2 \sim 100 \text{ kW/m}^2$ and gravity (g_x , g_y , g_z), have a certain theoretical guiding significance for the construction of the CSNS. The flow and heat transfer technology of supercritical liquid hydrogen in the U-tube inside the moderator determine the normal operation of the moderator. Based on the importance of flow and heat transfer technology of supercritical liquid hydrogen in the U-tube, the following conclusions could be obtained in the elbow:

1. During the flow of supercritical liquid hydrogen in U-tube, the heat transfer in the elbow part of the U-tube ($\alpha = 0^\circ \sim 180^\circ$) was strengthened, and heat transfer deterioration occurred at the elbow outlet ($\alpha = 180^\circ$ $L/D = 30$).
2. For the straight tube, when Re reached 1×10^5 , Nu approached to be constant. However, for the vertical elbow, when Re and q were from 27,375 to 54,750 and 80 kW/m^2 and 100 kW/m^2 , Nu increased by 56.6% and 3.7%, and Re had a more significant impact on Nu variation.
3. When the gravity direction was consistent with the flow direction of liquid hydrogen (g_x direction), the Nu number inside the channel was 4.21%, which is 5.56% higher than that in the g_y and g_z direction, respectively. The heat transfer capacity of fluid in flow channel along x -axis direction was the strongest, followed by the y -axis direction, and the z -axis direction was the weakest.

Author Contributions: W.F. and Y.L. (Yiping Lu) are the main authors of this manuscript. W.F., Y.L. (Yiping Lu), F.S., L.M., S.W., Y.L. (Youlian Lu), L.Z., S.F. and J.T. contributed to this manuscript. S.W. and J.T. proposed the research topic and gave the idea of the scheme. J.T. and Y.L. (Youlian Lu) analyzed the data and contributed analysis tools. L.Z. and J.T. designed the overall framework and provided guiding technical support. J.T. and L.M. checked, reviewed, and revised the paper. J.T. performed the final proofreading and supervised this research. All authors have read and agreed to the published version of the manuscript.

Funding: This research was supported by the Program for Guangdong Introducing Innovative and Enterpre-neurial Teams (project no. 2017ZT07S225), the National Natural Science Foundation of China (2017ZT07S225), the National Natural Science Foundation of China (Grant Nos. U1932219), the National Natural Science Foundation of China (No. 11805033) and State Key Laboratory of Nuclear Power Safety Monitoring Technology and Equipment (No. K-A2019.418).

Institutional Review Board Statement: Not applicable.

Informed Consent Statement: Not applicable.

Data Availability Statement: Not applicable.

Conflicts of Interest: The authors declare no conflict of interest.

Nomenclature

| | |
|--------------------------------|--|
| A | cross-sectional area: m^2 |
| D | tube hydraulic diameter, mm |
| δ | wall thickness, mm |
| τ | stress tensor |
| $\sigma_k, \sigma_\varepsilon$ | turbulent Prandtl numbers for k and ε |
| T | bulk fluid temperature, K |
| E | total energy, kJ/kg |
| P | static pressure, Pa |
| G_k, G_b | turbulence kinetic energy, $\text{kg}/\text{m}^2\text{s}$ |
| L | characteristic length, mm |
| R | curvature radius of the bend, mm |
| H | bulk liquid enthalpy, kJ/kg |
| Nu | Nussel number |
| Re | Reynolds number |
| T_w | averaging temperature of wall, K |
| T_b | bulk temperature of fluid, K |
| r | bend radius, mm |
| α | bending angle |
| k | turbulence kinetic energy, m^2/s^2 |
| p | bulk liquid pressure, Pa |
| u | velocity vector, m/s |
| h | heat transfer coefficient, $\text{W}/\text{m}^2\cdot\text{K}$ |
| ρ | density, kg/m^3 |
| λ | thermal conductivity of the fluid, $\text{W}/\text{m}\cdot\text{K}^{-1}$ |
| ε | dissipation rate of turbulent kinetic energy, m^2/s^3 |
| μ | dynamic viscosity, Pa·S |
| μ_t | turbulent viscosity, Pa·S |
| q_w | local heat flux of the wall, kW/m^2 |
| S_k, S_ε | source terms |
| ω | axial velocity, m/s |
| c_p | specific heat capacity, $\text{J}/\text{kg}\cdot\text{K}^{-1}$ |
| ν | kinematic viscosity, m^2/s |
| λ_{eff} | effective thermal conductivity, $\text{W}/\text{m}\cdot\text{K}^{-1}$ |
| τ_{eff} | shear stress, N/m^2 |
| S_h | volumetric heat source |

References

1. Chen, Z.J. China Spallation Neutron Source (CSNS). *J. Chin. Acad. Sci.* **2011**, *66*, 726–728.
2. Yin, W.; Liang, T.; Yu, Q. Neutronics design for the coupled para-hydrogen moderator for CSNS. *Nucl. Instrum. Methods Phys. Res. Sect. A Accel. Spectrometers Detect. Assoc. Equip.* **2011**, *631*, 105–110. [[CrossRef](#)]
3. Freels, J.D. COMSOL Validation Progress on Supercritical Hydrogen Heat Transfer. *Source* **2008**, *6*, 22–24.
4. Hu, J.; Li, Z.; Gao, Y.; Yang, J.; Liu, L. Investigation into Abnormal Heat Transfer Mechanism of Supercritical Carbon Dioxide in Vertically Upward Tube. *Chin. J. Ship Res.* **2021**, *16*, 170–179.

5. Aso, T.; Kaminaga, M.; Terada, A.; Hino, R. Thermal-Hydraulic Experiments and Analyses on Cold Moderator. In Proceedings of the ICANS-XV, Tsukuba, Japan, 11 November 2000; pp. 6–9.
6. Aso, T.; Monde, M.; Sato, H.; Hino, R.; Tatsumoto, H.; Kato, T. Experimental Investigation of Characteristics of Impinging Jet Heat Transfer and Application to JSNS Moderator Design. *Trans. At. Energy Soc. Jpn.* **2006**, *5*, 179–189. [[CrossRef](#)]
7. Hendricks, R.C.; Simon, F.F. Heat transfer to hydrogen flowing in a curved tube. *Chem. Prop.* **1963**, *7*, 7–9.
8. Beech, J.C. Forced Convection Heat Transfer to Supercritical Cryogenic Hydrogen: Part 1. *Lit. Surv.* **1969**, *12*, 47–50.
9. Zhou, B.; Ji, Y.; Sun, J.; Sun, Y.; Shi, L. Numerical Investigations of Supercritical Hydrogen Flow and Heat Transfer in Curved Tube. *Hedongli Gongcheng/Nucl. Power Eng.* **2019**, *40*, 197–201.
10. Ortiz, F.J.G.; López-Guirao, F.; Jiménez-Espadafor, F.J.; Benjumea, J.M. Heat Transfer Limitations in Supercritical Water Gasification. *Energies* **2022**, *15*, 177. [[CrossRef](#)]
11. Toor, S.S.; Shah, A.A.; Sharma, K.; Seehar, T.H.; Pedersen, T.H.; Rosendahl, L.A. Bio-Crude Production from Protein-Extracted Grass Residue through Hydrothermal Liquefaction. *Energies* **2022**, *15*, 364. [[CrossRef](#)]
12. Diao, L. Numerical Simulation of Flow and Heat Transfer Characteristics of Supercritical CO₂ in Straight and Spiral Tubes. Master's Thesis, Guangdong University of Technology, Guangzhou, China, 2020.
13. Zhang, K.; Han, C.; Ren, J.; Zhou, Y.; Bi, M. Numerical Simulation on Heat Transfer of Supercritical LNG in Coil Tubes of Submerged Combustion Vaporizer. *Huagong Xuebao/CIESC J.* **2015**, *66*, 4788–4795.
14. Yu, B.W.; Fan, Y.Y.; Wang, Y.S.; Hong, W.P.; Niu, X.J. Numerical study on heat transfer characteristics of supercritical CO₂-DME mixture in vertical circular tube. *Eng. Thermophys.* **2021**, *42*, 481–488.
15. Wang, Y.; Lu, Y.; Li, S.; Dong, M. Numerical Study on Heat Transfer of Supercritical-Pressure RP-3 Aviation Kerosene in U-Turn Circular Tubes. *Huagong Xuebao/CIESC J.* **2021**, *72*, 4639–4648.
16. Wu, M.T. *Numerical Study on Flow and Heat Transfer of n-Decane in Supercritical State*; Northeast Electric Power University: Jilin City, China, 2021.
17. Wu, X.M.; Zhao, R.; Wei, Z.F. Study on flow boiling heat transfer characteristics of CO₂/propane mixture in horizontal tube. *J. Eng. Thermophys.* **2013**, *34*, 4.
18. Keshavarzadeh, A.H.; Ahmadi, P.; Safaei, M.R. Assessment and Optimization of an Integrated Energy System with Electrolysis and Fuel Cells for Electricity, Cooling and Hydrogen Production Using Various Optimization Techniques. *Int. J. Hydrogen Energy* **2019**, *44*, 21379–21396. [[CrossRef](#)]
19. Han, C.L.; Ren, J.J.; Dong, W.P.; Bi, M.S. Numerical Investigation of Supercritical LNG Convective Heat Transfer in a Horizontal Serpentine Tube. *Cryogenics (Guildf)* **2016**, *78*, 1–13. [[CrossRef](#)]
20. Matsson, J.E. *An Introduction to ANSYS Fluent 2021*; SDS Publications: Mission, KS, USA, 2021; pp. 75–83.
21. Lemmon, E.; McLinden, M.O.; Huber, M.L. NIST Reference Fluid Thermodynamic and Transport Properties-REFPROP. *Chem. Prop.* **2002**, *23*, v7.
22. An, E.K.; Zhang, R.; Han, Y.F. Grid independence analysis of numerical simulation of multiphase turbulent combustion. *Boil. Technol.* **2018**, *49*, 5.
23. Friedman, R.; Graham, R.W.; Hendricks, R.C.; Hsu, Y.Y. Experimental Heat-Transfer Results for Cryogenic Hydrogen Flowing in Tubes at Subcritical and Supercritical Pressures to 800 Pounds per Square Inch Absolute. *Natl. Aeronaut. Space Admin.* **2016**, *16*, 1–23.
24. Zhu, L.; Lu, Y.; Tong, J.; Liang, T.; Lu, Y.; Fu, W.; Wang, B.; Zhang, Y. Sensitivity Analysis of Influencing Factors of Supercritical Methane Flow and Heat Transfer in a U-Tube. *Energies* **2021**, *14*, 5714. [[CrossRef](#)]
25. Mao, S.; Zhou, T.; Wei, D.; Liu, W.; Zhang, Y. Heat transfer characteristics of supercritical water in channels: A systematic literature review of 20 years of research. *Appl. Therm. Eng.* **2021**, *197*, 117403. [[CrossRef](#)]